Improved Seasonal Prediction of Rainfall over East Africa for Application in Agriculture: Statistical Downscaling of CFSv2 and GFDL-FLOR

O. KIPKOGEI

Intergovernmental Authority on Development Climate Prediction and Applications Centre, and Institute for Climate Change and Adaptation, University of Nairobi, Nairobi, Kenya

A. M. MWANTHI

Intergovernmental Authority on Development Climate Prediction and Applications Centre, Nairobi, Kenya

J. B. MWESIGWA

Intergovernmental Authority on Development Climate Prediction and Applications Centre, and Institute for Climate Change and Adaptation, University of Nairobi, Nairobi, Kenya

Z. K. K. ATHERU, M. A. WANZALA, AND G. ARTAN

Intergovernmental Authority on Development Climate Prediction and Applications Centre, Nairobi, Kenya

ABSTRACT

Statistically downscaled forecasts of October–December (OND) rainfall are evaluated over East Africa from two general circulation model (GCM) seasonal prediction systems. The method uses canonical correlation analysis to relate variability in predicted large-scale rainfall (characterizing, e.g., predicted ENSO and Indian Ocean dipole variability) to observed local variability over Kenya and Tanzania. Evaluation is performed for the period 1982–2011 and for the real-time forecast for OND 2015, a season when a strong El Niño was active. The seasonal forecast systems used are the National Centers for Environmental Prediction Climate Forecast System, version 2 (CFSv2), and the Geophysical Fluid Dynamics Laboratory Forecast-Oriented Low Ocean Resolution (GFDL-FLOR) version of CM2.5. The Climate Hazards Group Infrared Precipitation with Station Data (CHIRPS) rainfall dataset—a blend of in situ station observations and satellite estimates—was used at 5 km × 5 km resolution over Kenya and Tanzania as benchmark data for the downscaling. Results for the case-study forecast for OND 2015 show that downscaled output from both models adds realistic spatial detail relative to the coarser raw model output—albeit with some overestimation of rainfall that may have been derived from the downscaling procedure introducing a wet response to El Niño more typical of historical cases. Assessment of the downscaled forecasts over the 1982–2011 period shows positive long-term skill better than that documented in previous studies of unprocessed GCM forecasts for the region. Climate forecast downscaling is thus a key undertaking worldwide in the generation of more reliable products for sector specific application including agricultural planning and decision-making.

1. Introduction

The economy of East African nations and the livelihoods of many communities are largely dependent on rain-fed agriculture, which is highly vulnerable to the negative impacts of climate variability. Severe droughts

ⓐ Denotes content that is immediately available upon publication as open access.

Corresponding author: Oliver Kipkogei, oliver@icpac.net

and floods are recurrent hazards and frequently have a negative impact on the livelihoods of people in the region. On the continental scale, nearly one-third of the African population dependent on rain-fed food production face chronic food insecurity (Haile 2005; Washington and Downing 1999), with the main driver being weather and climate variability and agricultural production and food security. For the Greater Horn of Africa region, the drought of 2010/11, for example, affected some 13 million people with estimated deaths exceeding 50 000 (Hillier and Dempsey 2012). Weather

and climate forecasts have potential to provide early warning of climate hazards, enabling agricultural decision-makers to take mitigating actions to reduce losses and boost agricultural productivity and food security across the region. In this paper, we explore the potential for improving general circulation model (GCM)-based seasonal forecasts for the region using statistical postprocessing methodology based on canonical correlation analysis (CCA).

In recent years, there has been increasing demand for high-resolution climate forecasts at sufficient lead times to allow response planning from users in agriculture, hydrology, disaster management, and health, among others. GCM-based seasonal forecasts typically have low spatial resolution and to generate increased spatial detail, statistical or dynamical downscaling techniques are employed. In the dynamical technique, regional models, driven by initial and boundary conditions from GCMs, are used (Castro et al. 2006). This technique is the more fundamental in that it involves simulation of the dynamical and physical processes giving rise to spatial details. However, imperfect representation of such processes may introduce errors that limit the advantages (Milonov and Raschendorfer 2001). In addition, the dynamical approach is costly in terms of computing resources and associated science and technical support. In contrast, statistical downscaling methods use an empirical approach based on comparing a target set of historical observations with corresponding retrospective forecasts to develop a statistical model that identifies relationships between the coarse-resolution GCM and the higher-resolution observational data (Wilby et al. 1998). This technique has been shown to be effective (Ndiaye et al. 2009) and demands minimal computing facilities. In this paper, we use a statistical approach based on CCA.

Processed output from GCMs has been used to aid understanding and prediction of weather and climate in the region for a range of time scales. For example, Kipkogei et al. (2016) combined global output products from four centers using the multimodel superensemble technique and noted that it greatly reduced errors in forecasts for the day 1–10 range. Rowell et al. (2016) investigated potential for evaluating the trustworthiness of GCM climate change projections based on their performance for simulating present-day climate, with the aim of disregarding or down weighting poorer performing models. It was found that this processing was unhelpful in reducing the wide dispersion in model projected rainfall and temperature changes. Rowell et al. (2015) noted that the March–May rains in the region have exhibited a downward trend in recent decades, whereas most major global climate models project an increasing trend for the coming decades, a phenomenon termed the East African climate paradox.

Rainfall prediction in the eastern Africa region is usually derived from several oceanic and atmospheric features related to the seasonal rainfall. Regional rainfall teleconnections with global ocean sea surface temperature (SST) patterns associated with El Niño–Southern Oscillation (ENSO) and the Indian Ocean dipole (IOD) as well as SST gradients have been utilized extensively for seasonal rainfall prediction (Mutai et al. 1998; Saji et al. 1999; Indeje et al. 2000; Marchant et al. 2007; Gitau et al. 2015; Owiti et al. 2008; Terray and Dominiak 2005; Smith et al. 2007; Kumar et al. 1999) with most success for the "short rains" season (relative to the March–May "long rains"). Other authors have investigated preseason atmospheric variables as predictors. For example, Nicholson (2014) found that atmospheric variables generally provide higher forecast skill than surface variables such as sea surface temperatures. The rainfall seasonality in the region is also modulated by circulations associated with the intertropical convergence zone (Okoola 1999; Nicholson 2003; Donohoe et al. 2013). Other systems that can influence regional rainfall include the East Africa low-level jet stream and the Indian Ocean subtropical high pressure cells (Gitau et al. 2015), winds and local factors (Johansson and Chen 2003), as well as secondary effects resulting from tropical cyclone activities (Shanko and Camberlin 1998), among other factors.

Since 1998, the Intergovernmental Authority on Development (IGAD) Climate Prediction and Applications Centre (ICPAC) has been spearheading the generation of regional seasonal forecasts for the Greater Horn of Africa (GHA). The forecasts are an output of the GHA Climate Outlook Forum (GHACOF) process and are developed as a consensus product with the National Meteorological and Hydrological Services (NMHSs) of the 11 constituent GHA countries. Probability forecasts of 3-month rainfall totals are provided with typically 1-month lead time [e.g., the forecast for October–December (OND) is issued in late August]. The consensus provides a regional context that NMHSs may employ to assist production of national downscaled forecasts.

This paper is part of an ongoing work on the generation of improved downscaled monthly and seasonal forecasts to promote food security initiatives at both national and farming community levels over East Africa. Although objective use of seasonal-time-scale GCM outputs for the region is increasing, it is not yet fully implemented into operational practice, and it is therefore timely to evaluate their potential benefits, particularly after postprocessing with the CCA technique discussed.
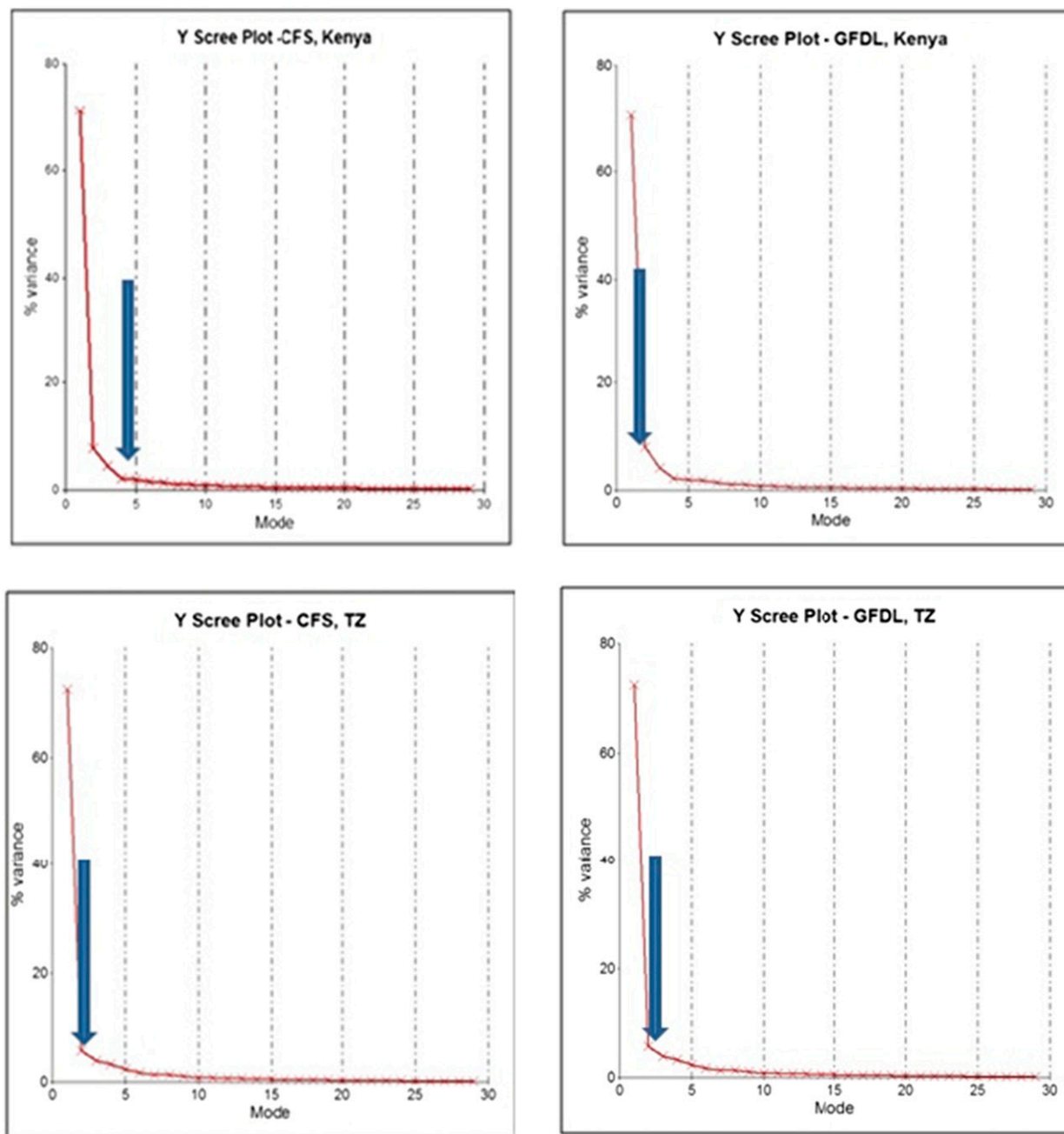
FIG. 1. Percentage of variance explained by *Y* modes over (top) Kenya and (bottom) Tanzania with (left) CFS and (right) GFDL.

2. Area of study

To evaluate the CCA technique, we focus on Kenya and Tanzania, two countries that make up a substantial part of the equatorial and southern GHA; however, the method may be readily applied to other countries. Kenya lies within 5.2°S–5.1°N latitude and 33.5°–42.3°E longitude, whereas Tanzania lies within 12.3°–0.4°S latitude and 28.7°–41°E longitude. Rainfall in much of

this region exhibits a bimodal cycle with most rainfall in March, April, and May (the long rains season) as the ITCZ moves north and in October, November, and December (the short rains season) as it moves south.

3. Data

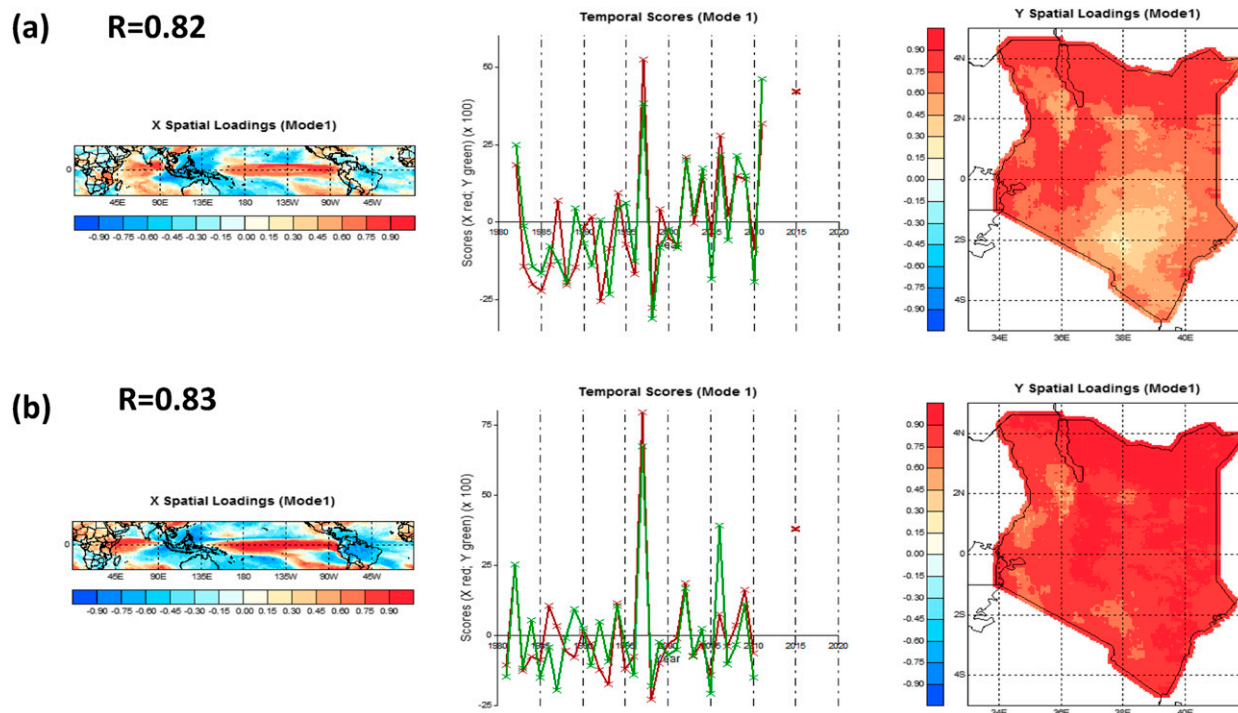This study utilized rainfall hindcasts and forecasts from two global seasonal forecasting systems, namely, the

FIG. 2. First CCA paired mode (mode 1) for (a) CFSv2 and (b) GFDL-FLOR over Kenya: (left) X spatial loadings; (right) Y spatial loadings; (center) temporal scores over the 1982–2011 hindcast period and for the 2015 forecast (X pattern).

National Centers for Environmental Prediction (NCEP) CFSv2 and the Geophysical Fluid Dynamics Laboratory Forecast-Oriented Low Ocean Resolution (GFDL-FLOR) version of CM2.5. Forecasts from both systems contribute to the North American Multimodel Ensemble (NMME) for seasonal forecasting (Kirtman et al. 2014). Observed gridded rainfall data from the high-resolution Climate Hazards Group Infrared Precipitation with Station Data (CHIRPS) dataset are used in downscaling procedures and for forecast verification.

NCEP CFSv2 is a coupled global model with a resolution of 0.937° (T126) with 24 ensemble members (Saha et al. 2006, 2010, 2014). CFSv2 has a spectral triangular truncation of 126 waves in the horizontal and a finite differencing in the vertical with 64 sigma pressure hybrid layers (Saha et al. 2014) with an interactive three-layer sea ice model, an upgraded four-level soil model, and a prescribed historical carbon dioxide concentrations (Wu et al. 2005) and parameterization of mountain blocking (Alpert 2004; Lott and Miller 1997).

GFDL-FLOR is an improved version of the GFDL Climate Model, version 2.5 (CM2.5; Delworth et al. 2012), and GFDL Climate Model, version 2.1 (CM2.1; Delworth et al. 2006), with 12 ensemble members and 32 vertical atmospheric levels (Vecchi et al. 2014). It has been used extensively to simulate precipitation and temperature over

land (Jia et al. 2015) as well as drought patterns (Delworth et al. 2015). GFDL-FLOR has a land and atmospheric resolution of 0.45° and an ocean resolution of 1°.

The CHIRPS dataset, a blend of station rainfall data and satellite estimates from the Climate Hazards Group (Funk et al. 2015), was used as training data for the forecast downscaling as well as for forecast verification. The methodology for blending satellite estimates and station data is explained in detail in Funk and Verdin (2010).

4. Methodology

In this study, the climate predictability tool (CPT) software developed by the International Research Institute for Climate and Society (Mason and Tippett 2017) was used to statistically downscale the GCM rainfall forecasts. Climate downscaling bridges the gap in the spatial scale of the global climate models and the resolution needed to carry out assessment of potential local-scale impacts. When local and large-scale forecast variables exhibit a linear relationship, and are normally distributed, a regression is the best method for downscaling (Yun et al. 2003; Wilby et al. 2002; Zheng and Renwick 2003; Feddersen and Andersen 2005; Kang et al. 2007; Kang et al. 2009). With statistical downscaling, there is a target set of observations (for this case,
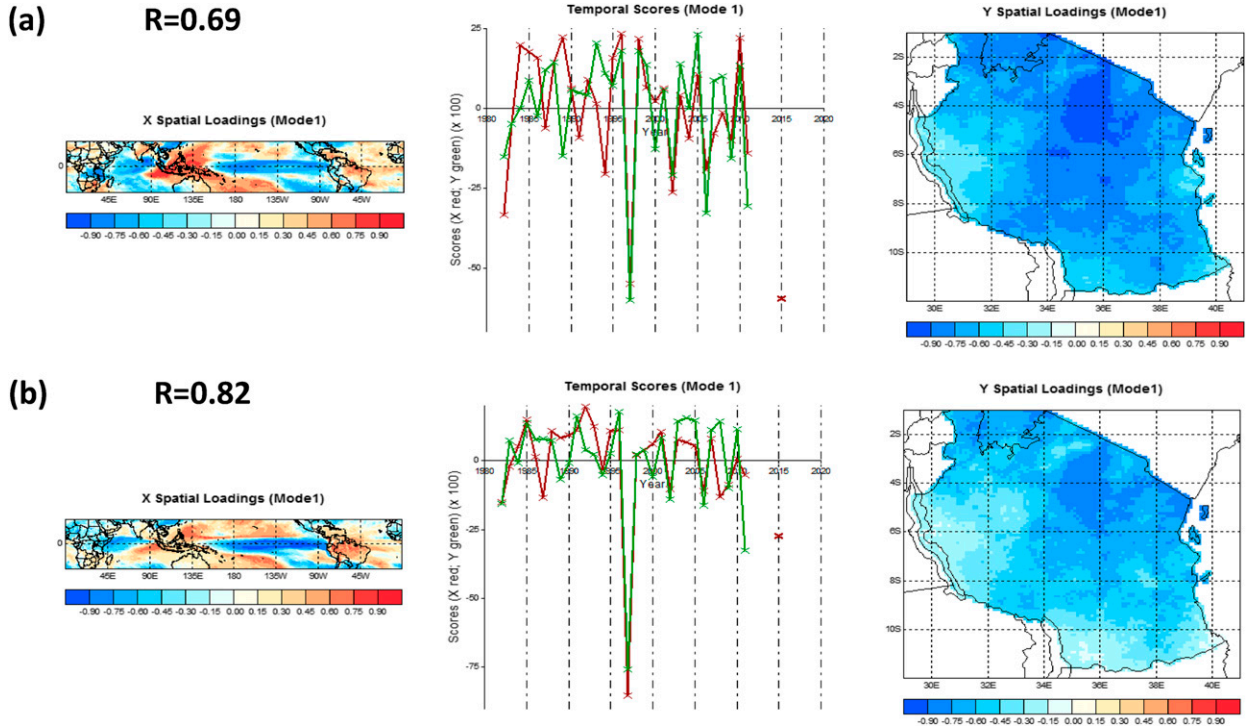
FIG. 3. As in Fig. 2, but for Tanzania.

CHIRPS) and the statistical model identifies statistical relationships between the coarse-resolution GCM and the corresponding observational data over the target region. In this case, retrospective forecasts for OND over the period 1982–2011 were used in cross-validated mode (e.g., Michaelsen 1987) to develop the statistical models.

CCA is a multivariate statistical technique that seeks to decompose covariability in two sets (X, Y) of spatio-temporal data into a series of orthogonal paired patterns (CCA modes) that have maximum linear correlation over associated time series of X and Y projections on their corresponding modes. The modes are ranked according to the magnitude of the time series correlation (Wilks 2006, 1995; Tatsuoka 1988; Chu and He 1994). CCA has the ability to detect and correct bias in amplitude, mean, and shape of anomaly patterns when trained on hindcast data and corresponding observations and thus may be used both to calibrate model outputs as well as increase spatial detail in forecasts (Mason and Tippett 2016; Mason and Mimmack 2002). Maximization of the linear correlation is well suited to prediction problems since the procedure seeks to identify the strongest possible relationship between predictors and predictands. In the application of CCA available in CPT, predictors (X) and predictands (Y) are pre-orthogonalized separately using a standard empirical orthogonal function (EOF)

analysis. A limited number of these EOF time series are then used in the CCA procedure. The CCA modes are determined based on the covariability of the truncated predictor and predictand EOF time series in the training period. The predictor data are then projected onto the CCA loading patterns to generate forecasts.

The CCA technique can be summarized mathematically following Wilks (1995, 2006). Given two variables x and y of same time dimension, a determination on their degree of association can be made by constructing two canonical variates CV_{x1} and CV_{y1}:

$$CV_{x1} = a_1 x_1 + a_2 x_2 + a_3 x_3 + \ldots + a_n x_n \quad \text{and} \quad (1)$$

$$CV_{y1} = b_1 y_1 + b_2 y_2 + b_3 y_3 + \ldots + b_m y_m. \quad (2)$$

In Eqs. (1) and (2), $a_1, \ldots, a_n$ and $b_1, \ldots, b_m$ are the canonical weights selected to maximize the degree of association between the variates. The first pair of the canonical weighting factors maximizes the degree of relationship (correlation) over all possible weights. The second pair is selected using the same criteria, with the additional requirement that the time series of weights is not correlated with those of the first pair. The time series of weights for the third pair are selected to be uncorrelated with the first and second pair, and so on (Barnston and Ropelewski 1992; Cherry 1996; Repelli and Alves 1996; Nicholls 1987). Comparison with other
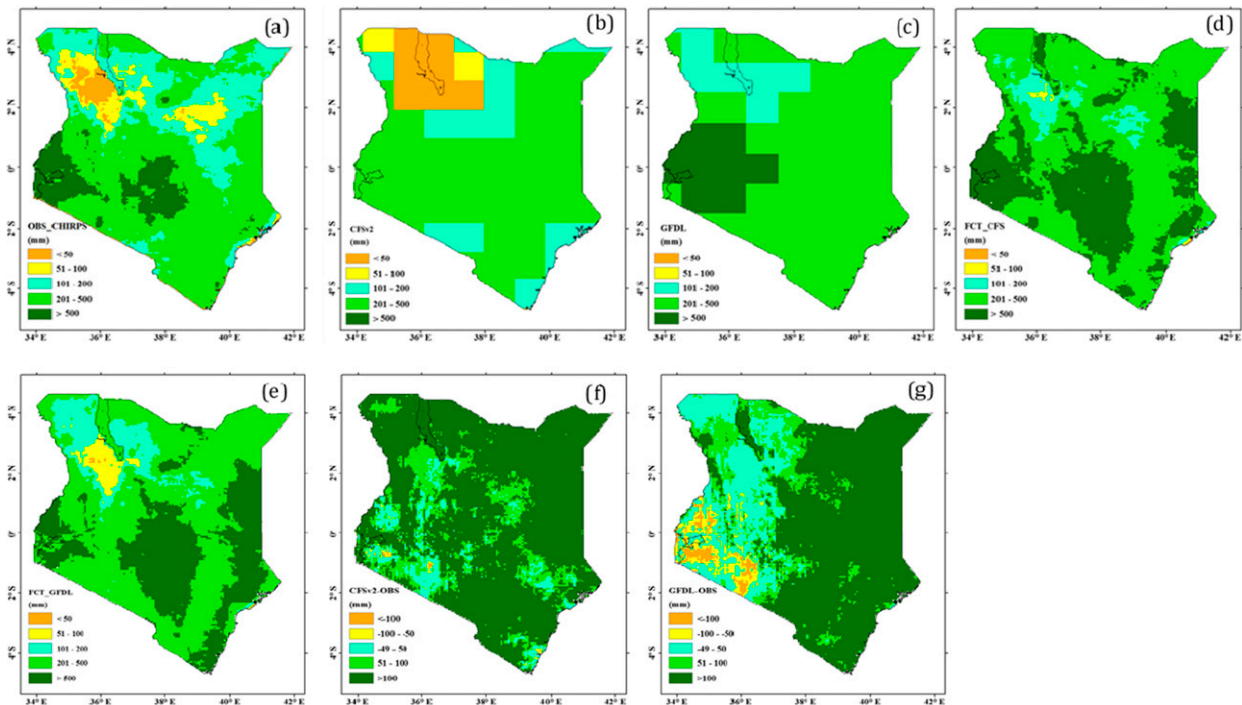
FIG. 4. Observed and predicted OND 2015 rainfall (mm) over Kenya: (a) observed rainfall (CHIRPS), raw (undownscaled) predictions from (b) CFSv2 and (c) GFDL-FLOR, downscaled predictions from (d) CFSv2 and (e) GFDL-FLOR, and the departures of downscaled forecasts from observations for (f) CFSv2 and (g) GFDL-FLOR.

downscaling methods has been explained in detail (Liu et al. 2015; Wilby and Wigley 1997).

In the following section, assessments of deterministic forecasts for OND 2015 and probabilistic forecasts of rainfall tercile categories over the hindcast period are made. Probability forecasts are generated in the CPT package by constructing a probability density function (PDF) for each data point, with mean equal to the deterministic output of the CCA analysis and standard deviation given by the mean error of the downscaled forecasts. Probabilities for tercile categories are then derived from the PDF.

In the CCA configurations used, a circumtropical X domain (30°S–30°N and 0°–359°E) is employed. The X variable employed is the ensemble mean predicted precipitation for the OND target season. The circumtropical X domain was selected to harness teleconnection responses to the East African region from large-scale climate modes, predominantly ENSO and IOD, while use of precipitation as the predictor variable should characterize the large-scale convective heating associated with the transmission of teleconnection effects associated with these climate modes. Shukla et al. (2014) have used a similar domain in a constructed analog approach to predict March–May rainfall over a subregion of East Africa. The Y domains

used are defined by the Kenyan and Tanzanian national boundaries, with a separate analysis performed for each country. The CFSv2 and GFDL-FLOR OND forecasts used as X (predictor) fields were initialized in September.

Scree plots that explain the percentage of variance associated with each X and Y EOF were used to determine the number of modes used to make cross-validated forecasts. Modes were selected based on identification of "elbows" in the scree plots with numbers chosen extending up to and not including the elbows (Mason and Graham 2002). For CFSv2, for example, for the Y variable, 4 and 2 modes were used over the Kenyan and Tanzanian domains, respectively, explaining a cumulative variance > 70% (Fig. 1). Over the Kenya domain, for example, the CFSv2 times the spatial loading pattern for CCA mode 1 (Fig. 2a) shows a classic positive ENSO (El Niño) and a positive IOD pattern. The paired Y spatial loading for mode 1 shows that the X pattern is related to above-normal precipitation over the whole of the Y (country) domain, with the highest loadings in the north and west. The temporal scores show how much each pattern was evident in past years. For example, both the X and Y patterns have high scores in 1997 when positive ENSO and IOD occurred and the rainfall was well above normal. The X temporal score for 2015 is
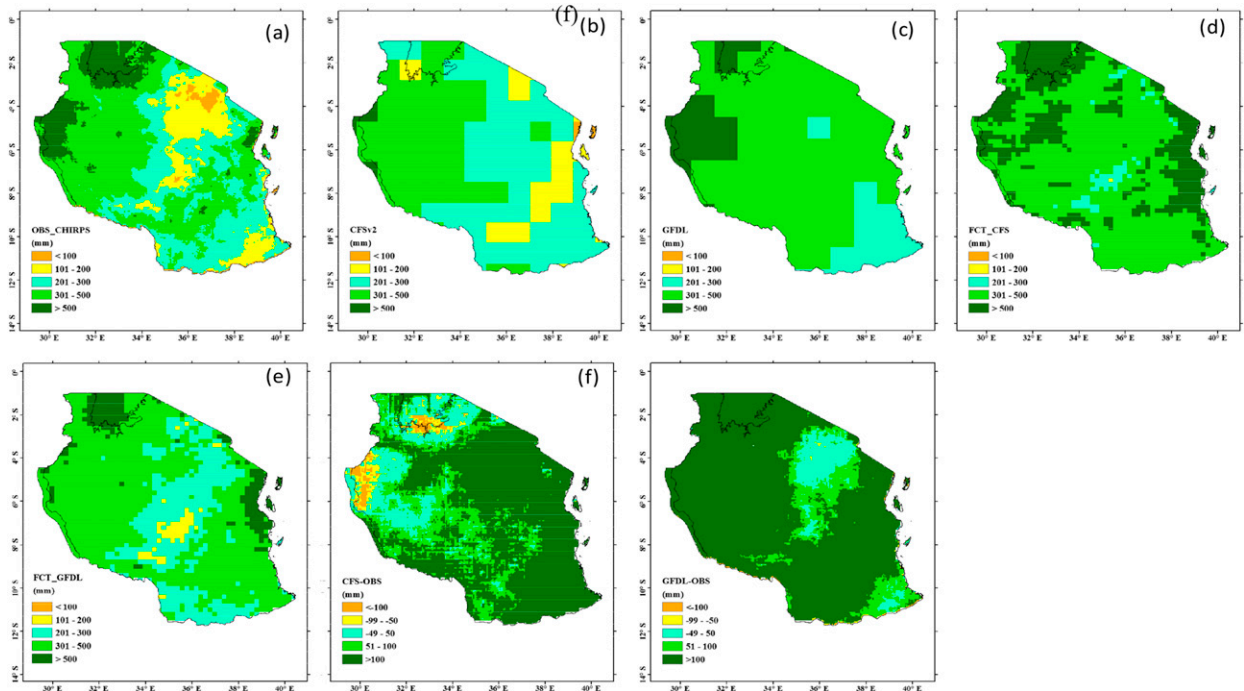
FIG. 5. As in Fig. 4, but for Tanzania.

similar to that of 1997—indicating that the forecast signals a similarly wet outcome. Results are similar for GFDL (Fig. 2b), though with a lower temporal score for the 2015 forecast relative to 1997. Similar X and Y loading patterns are found for the Tanzania analysis (Fig. 3—note the color convention is reversed from that of Fig. 2), with again the CFSv2 system being more confident of a 2015 outcome similar to that of 1997 than the GFDL system.

We evaluate the forecast performance over the 1982–2011 period using the World Meteorological Organization (WMO) standard forecast verification scores. These include the relative operating characteristics (ROC) curve and area under the curve (ROC score), the latter being recognized as an equivalent to the Hanssen–Kuipers skill score (KSS) when applied to deterministic forecasts (Hanssen and Kuipers 1965, Swets 1973; Mason 1982; Harvey et al. 1992; Mason and Graham 1999; Mason and Chidzambwa 2008). ROC is a measure of the quality of the forecasts that relates the hit rates and false alarm rates associated with predicting a given event (e.g., rainfall below the lower tercile). To calculate the ROC, the event is deemed forecast if its predicted probability exceeds a threshold value.

Hit rates and false-alarm rates are calculated for a range of forecast probability thresholds and are typically plotted to form a curve on an ROC diagram of hit rates (Y axis) versus false-alarm rates (X axis). For a skillful forecast, hit rates must exceed false-alarm rates, and the ROC curve will bulge upward from the diagonal and have a normalized area under the curve greater than 0.5; the more so, the greater is the forecast skill. Forecasts that have an ROC curve located on or near the diagonal (ROC score of order 0.5) effectively have hit rates equal to false-alarm rates and have no ability to discriminate the event from the nonevent (Mason and Graham 2002; Kharin and Zwiers 2003). Mason and Weigel (2009) have shown that the ROC score may be interpreted as the percentage of forecasts that correctly discriminate the forecast event from the nonevent.

5. Results and discussion

a. Real-time forecast for OND 2015

Figures 4 and 5 show observed, raw, and downscaled model forecasts (CFSv2 and GFDL-FLOR) for OND 2015 over Kenya and Tanzania, respectively. For the downscaled forecasts, the deviation from observations is also shown. Kenya and the northern part of Tanzania basically lie within the equatorial belt and are associated with a wet signal in OND when ENSO is in its positive phase. Over Kenya, downscaled forecasts from both CFSv2 and GFDL-FLOR (Figs. 4d,e) indicated that most parts would receive amounts of between 200 and 500 mm, with some parts in western, central, and eastern
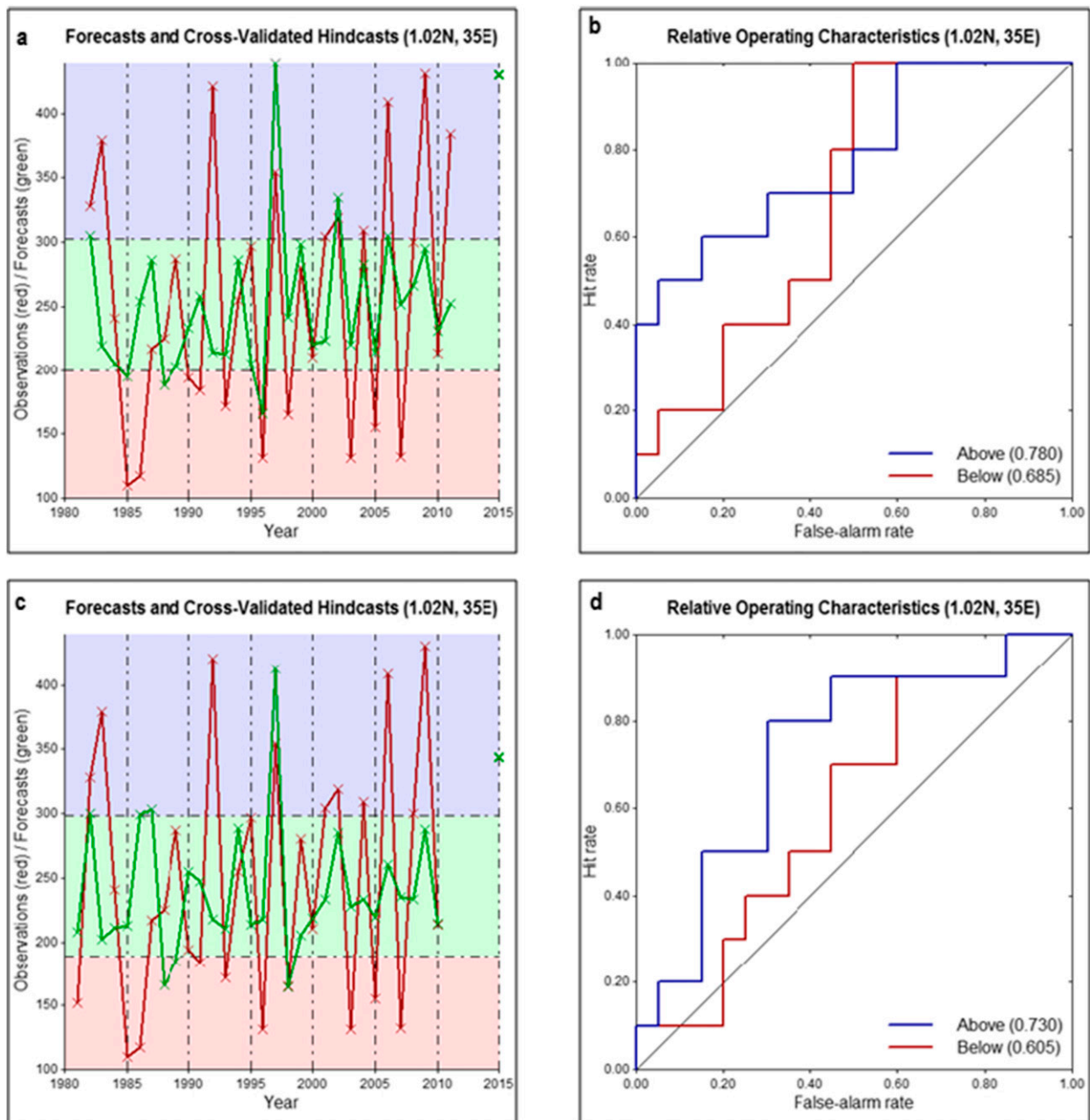
FIG. 6. Forecasts and cross-validated hindcasts for the location 1.02°N, 35°E (Kitale area in Kenya) for the OND 2015 season for (a) CFSv2 and (c) GFDL-FLOR, along with ROC scores for the same location for (b) CFSv2 and (d) GFDL-FLOR. ROC scores are calculated over the hindcast period 1982–2011 using a cross-validation window of 3 yr.

Kenya expected to receive rains greater than 500 mm. The downscaled GFDL (Fig. 4e) improves on the raw GFDL (Fig. 4c) by better capturing rainfall amounts and distribution in the drier area in the northwest as well as the wetter area in central Kenya. This improvement is also apparent, though to a lesser degree, with the CFSv2 downscaled forecast (Fig. 4d). The computed difference between the downscaled forecasts of both models and

observations (Figs. 4f,g) shows that both models over-forecast in the eastern parts of Kenya. In contrast, the GFDL model underforecast rainfall amounts around the Lake Victoria basin by more than 100 mm in some places (Fig. 4g). Over other parts of western Kenya, GFDL-FLOR gave the better performance with small departures from observations (±50 mm) more wide-spread than for CFSv2.
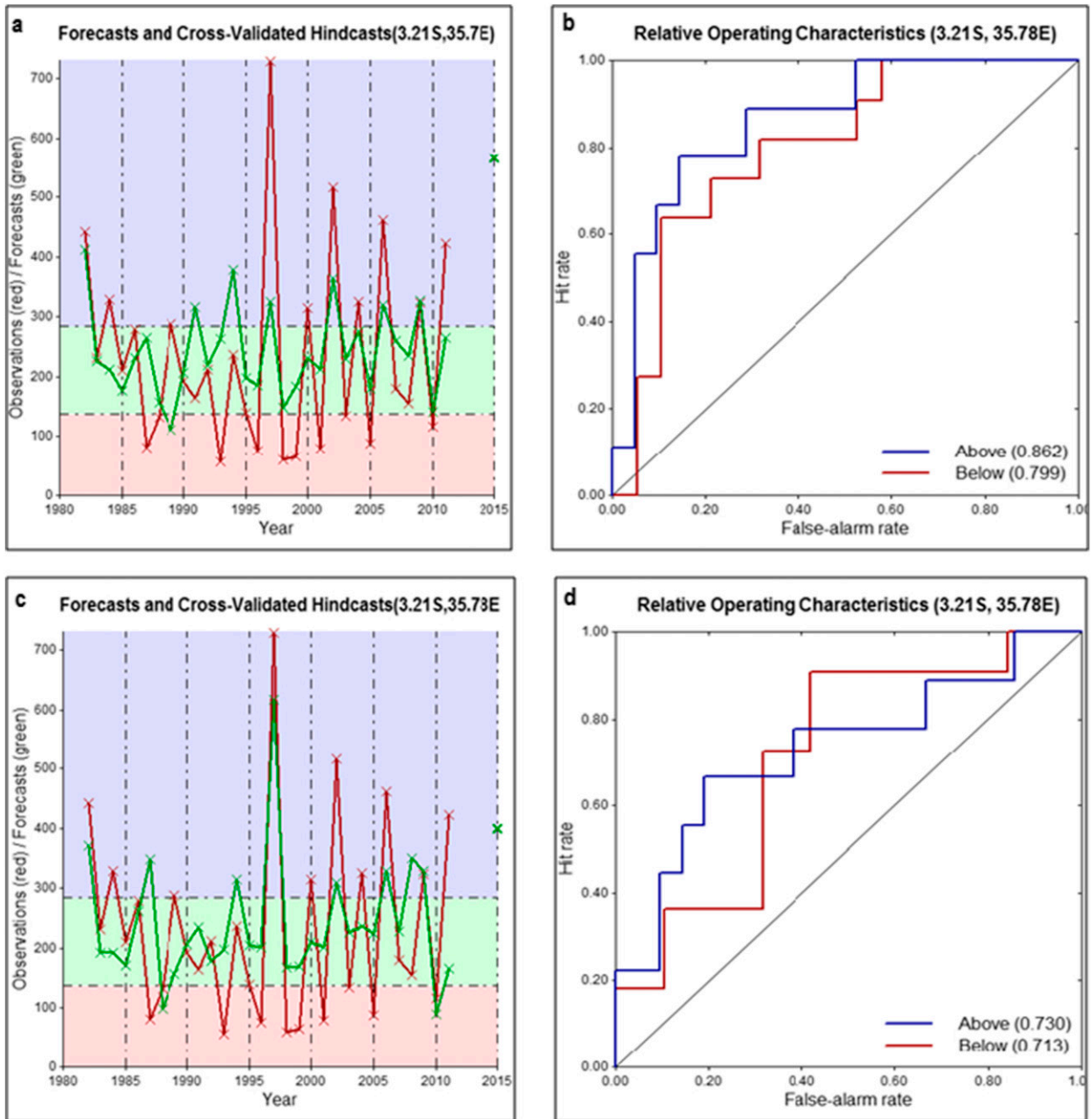
FIG. 7. As in Fig. 6, but for the location 3.21°S, 35.78°E (Arusha area in northern Tanzania).

Results for Tanzania are provided in Fig. 5. The downscaled forecasts (Figs. 5d,e) indicated that most parts would receive amounts greater than 300 mm for both the CFSv2 and GFDL-FLOR. Raw forecasts from the CFSv2 model (Fig. 5b) underforecast rains in the northern and western parts of the country, and these wet peaks are much better captured by the downscaled CFSv2 (Fig. 5d). In these areas CFSv2 performed better than GFDL-FLOR, as may be seen by comparing the corresponding deviations from observations (Figs. 5f,g), which show overprediction

by GFDL-FLOR by more than 100 mm. Indeed GFDL-FLOR overforecast over much of the country except on the central region, while in CFSv2 overforecasting was limited to the eastern half of Tanzania.

b. Hindcast skill assessment

Skill scores in terms of ROC and correlation were computed to gauge the skill of the downscaled forecasts with a cross-validation window of 3 yr. Figures 6 and 7 show cross-validated hindcasts and ROC scores for
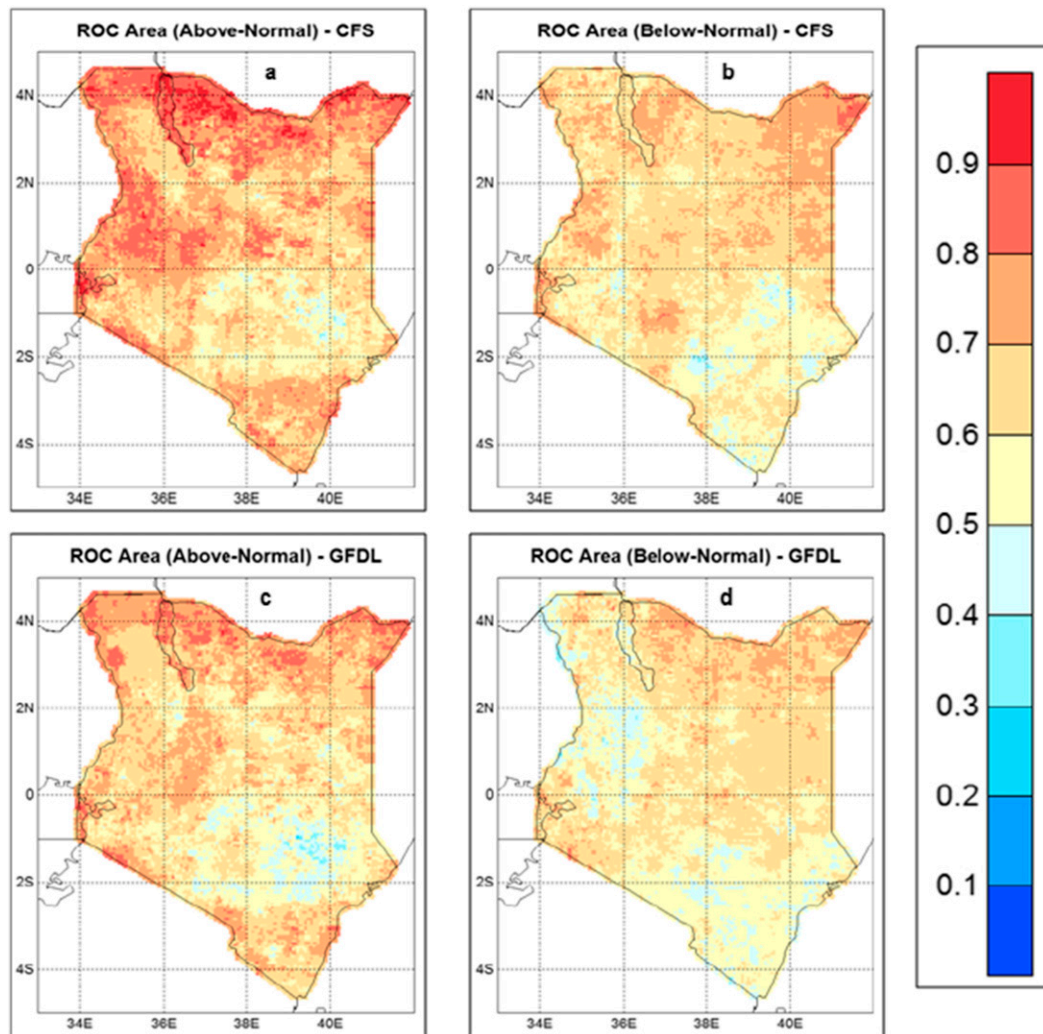
FIG. 8. ROC scores (area under curve) for the OND 2015 season for the (left) above- and (right) below-normal tercile rainfall forecast categories for Kenya from (a),(b) the CFSv2 system and (c),(d) the GFDL-FLOR system. ROC scores are calculated over the hindcast period 1982–2011 using a cross-validation window of 3 yr and plotted on the CHIRPS grid.

a location in Kenya (Kitale area; 1.02°N, 35°E) and Tanzania (Arusha area; 3.21°S, 35.78°E) for the CFSv2 (Figs. 6a,b and 7a,b) and GFDL-FLOR (Figs. 6c,d and 7c,d), respectively. Both areas form important agricultural belts for the two countries. ROC scores for Kitale and Arusha stations indicate that CFSv2 had scores of 0.78 (0.69) and 0.86 (0.80), respectively, whereas the GFDL-FLOR had scores of 0.73 (0.61) and 0.73 (0.71) for the above-normal (below normal) forecast categories. This implies that the models presented are skillful in capturing categorical forecasts in the given locations.

Figures 8 and 9 show the spatial distribution of ROC scores over Kenya and Tanzania, respectively. The figures show that most areas over the two countries had ROC values greater than 0.5 with coherent areas present

with scores exceeding 0.7, most notably for predictions of the above-normal category. Indeed, the ROC scores for the above-normal category for both models reach 0.8 locally for parts of northern and western Tanzania and northern and western parts of Kenya. In such regions, the downscaled forecasts correctly discriminate the observed category on 80% of the occasions (Mason and Weigel 2009). Figure 10 shows the Pearson correlation scores for the OND season for both CFSv2 (Figs. 10a,b) and GFDL-FLOR (Figs. 10c,d) over Kenya and Tanzania. Pearson correlation gauges the strength of association between two variables. Most parts of Kenya have correlation scores greater than 0.45 with the highest scores of greater than 0.75 being recorded in the northeastern parts for both CFSv2 and GFDL-FLOR. Most areas of
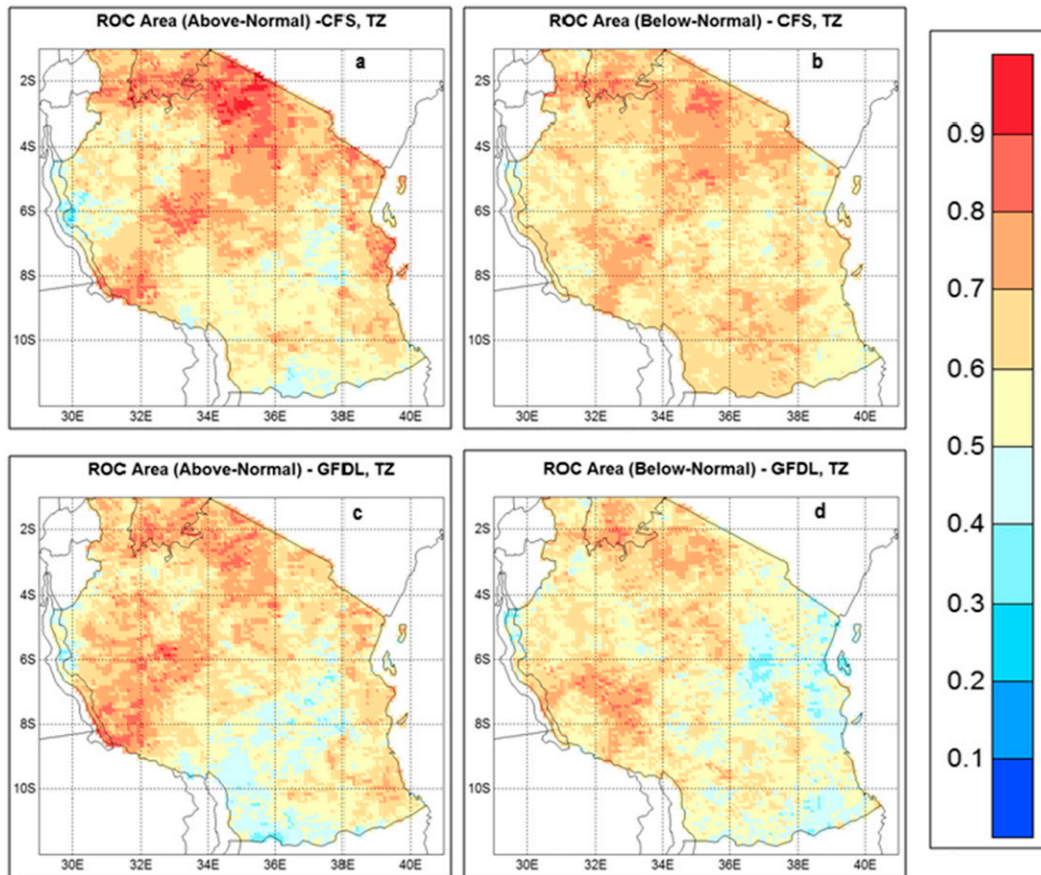
FIG. 9. As in Fig. 8, but for Tanzania.

Tanzania had scores of between 0.15 and 0.3, with an exception of a few patches in northern parts that had a score greater than 0.45 for both models. These correlation scores are similar or better than those found by other authors using unprocessed GCM output, indicating that the improved spatial detail does not come at the expense of reduced skill. For example, Mwangi et al. (2014) found correlations of between 0.4 and 0.7 for climatic zones of Kenya and correlations of less than 0.3 for much of Tanzania from September-initialized ECMWF System 4 forecasts. The relatively low scores obtained over southern Tanzania relative to northern parts and Kenya in this study are likely related to rainfall seasonality: OND is a wet season in the north of the country (and Kenya), but this period largely precedes the key wet season, December–February, over central and southern parts of Tanzania.

6. Conclusions

Weather and climate downscaling is an important area for both research and applications. Currently, a number of techniques are being tested and proposed for use in translating coarse climate forecasts into finer resolutions for improved decision-making. Statistical downscaling using the climate predictability tool is one of these techniques.

This study utilized forecast products from two seasonal forecast systems, namely, the NCEP CFSv2 and the GFDL-FLOR, calibrated using the high-resolution blended CHIRPS rainfall dataset. The ROC performance metric and Pearson correlation were used for evaluating downscaled hindcasts for the OND season. Evaluation was performed for the period 1982–2011 and for the real-time forecast for OND 2015 for the downscaled forecasts. Although evaluation was not done for the raw forecasts over the hindcast period, the raw OND 2015 was generated for comparison purposes.

The main findings of this study show that downscaled forecasts from both models had good skill in estimating seasonal rainfall amounts. In the 2015 case study, the downscaled fields from both models were found to add useful spatial detail relative to the coarser raw model output extracted for the same regions. In particular, the observed relatively wet conditions over central and western Kenya and dry conditions in northwest Kenya were well delineated. In general, the downscaled forecasts for this case overestimated rainfall in many parts of both
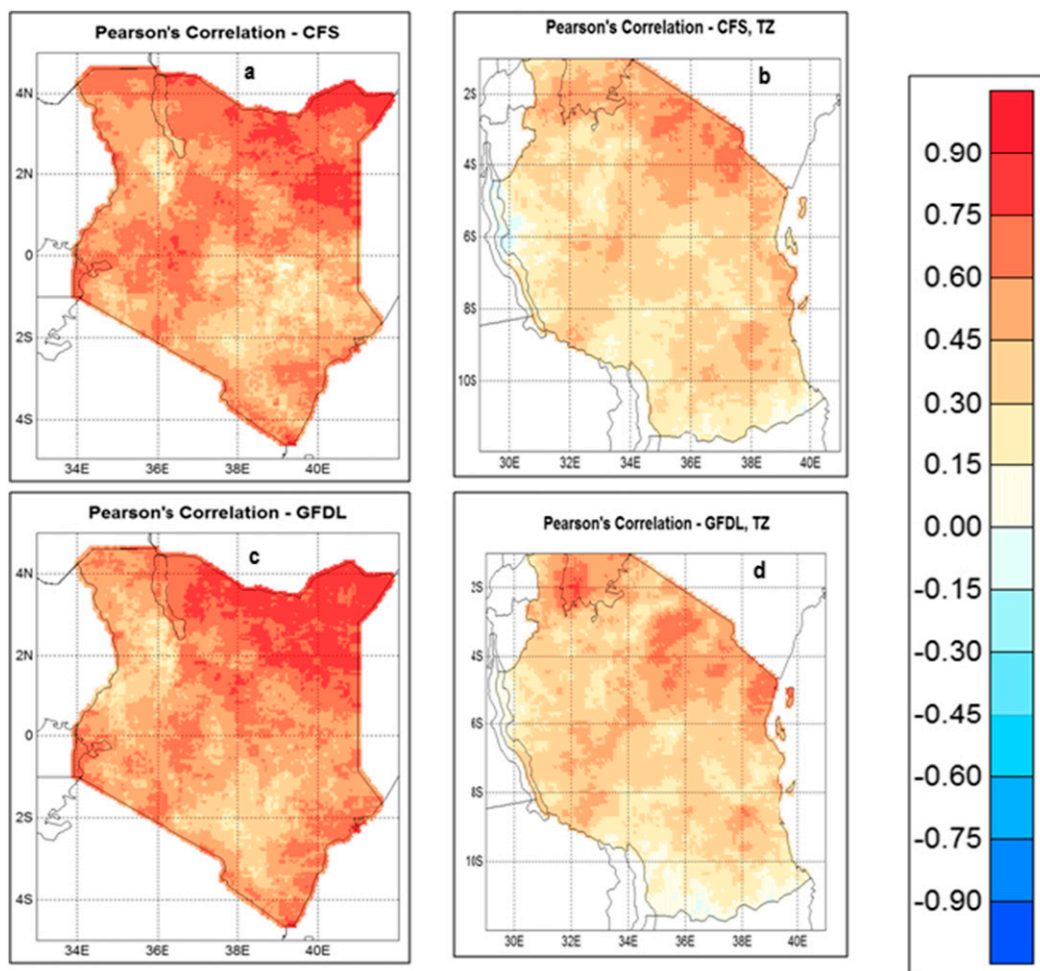
FIG. 10. Pearson correlation scores for the OND 2015 season for (a),(b) CFSv2 and (c),(d) GFDL-FLOR for (left) Kenya and (right) Tanzania. Correlation scores are calculated over the hindcast period 1982–2011 using a cross-validation window of 3 yr.

countries, particularly in the east—perhaps because the use of a circumtropical predictor field introduced a more typical wet response to the El Niño forcing than was actually observed in 2015. Notwithstanding, the overprediction in some parts of the region for OND 2015, assessment of the downscaled forecasts over the 1982–2011 period shows positive long-term skill similar to or better than that documented in other studies of skill for unprocessed GCM output. Probabilistic forecasts correctly discriminate the above-normal tercile category more than 70% of the time over substantial areas, particularly in northern Kenya and central–eastern Tanzania. The ability to discriminate the below-normal category is somewhat weaker, though it is achieved in more than 60% of the forecasts over much of the area.

Most parts of Kenya had Pearson correlation scores greater than 0.45, with highest scores of greater than 0.75 being recorded in northeastern parts. Most of the areas

in central and southern Tanzania had a score of between 0.15 and 0.3, with an exception of a few patches in the northern parts that had a score greater than 0.45. Lower scores in southern Tanzania may reflect the fact that, in this region, the OND period does not correspond with a rainy season peak as in the north.

Reliable climate information plays a vital role in policy formulation and improved decision-making. This paper therefore promotes generation of improved downscaled forecasts for application in food production programming and decision-making both at the national and farming community levels. Further research and work are needed to improve the existing downscaling techniques and propose new ones in order to further improve quality of forecast products.

REFERENCES

Alpert, J. C., 2004: Subgrid-scale mountain blocking at NCEP. *20th Conf. on Weather Analysis and Forecasting*, Seattle, WA, Amer. Meteor. Soc., P2.4, https://ams.confex.com/ams/pdfpapers/71011.pdf.

Barnston, A. G., and C. Ropelewski, 1992: Prediction of ENSO episodes using canonical correlation analysis. *J. Climate*, **5**, 1316–1345, https://doi.org/10.1175/1520-0442(1992)005<1316:POEEUC>2.0.CO;2.

Castro, C. L., R. A. Pielke Sr., and G. Leoncini, 2006: Dynamical downscaling: assessment of value retained and added using the regional atmospheric modeling system (RAMS). *J. Geophys. Res.*, **110**, D05108, doi:10.1029/2004JD004721.

Cherry, S., 1996: Singular value decomposition and canonical correlation analysis. *J. Climate*, **9**, 2003–2009, https://doi.org/10.1175/1520-0442(1996)009<2003:SVDAAC>2.0.CO;2.

Chu, P. S., and Y. He, 1994: Long-range prediction of Hawaiian winter rainfall using canonical correlation analysis. *Int. J. Climatol.*, **14**, 659–669, https://doi.org/10.1002/joc.3370140605.

Delworth, T. L., and Coauthors, 2006: GFDL's CM2 global coupled climate models. Part I: Formulation and simulation characteristics. *J. Climate*, **19**, 643–674, https://doi.org/10.1175/JCLI3629.1.

——, and Coauthors, 2012: Simulated climate and climate change in the GFDL CM2.6 high-resolution coupled climate model. *J. Climate*, **26**, 2766–2781, https://doi.org/10.1175/JCLI-D-11-00316.1.

——, F. Zeng, A. Rosati, G. A. Vecchi, and A. T. Wittenberg, 2015: A link between the hiatus in global warming and North American drought. *J. Climate*, **28**, 3834–3845, https://doi.org/10.1175/JCLI-D-14-00616.1.

Donohoe, A., J. Marshall, D. Ferreira, and D. McGee, 2013: The relationship between ITCZ location and cross equatorial atmospheric heat transport: From the seasonal cycle to the Last Glacial Maximum. *J. Climate*, **26**, 3597–3618, https://doi.org/10.1175/JCLI-D-12-00467.1.

Feddersen, H., and U. Andersen, 2005: A method for statistical downscaling of seasonal ensemble predictions. *Tellus*, **57A**, 398–408, https://doi.org/10.3402/tellusa.v57i3.14656.

Funk, C., and J. P. Verdin, 2010: Real-time decision support systems—The Famine Early Warning System network. *Satellite Rainfall Applications for Surface Hydrology*, M. Gebremichael and F. Hossain, Eds., Springer, 296–320.

——, A. Verdin, J. Michaelsen, P. Peterson, D. Pedreros, and G. Husak, 2015: A global satellite assisted precipitation climatology. *Earth Syst. Sci. Data*, **7**, 275–287, https://doi.org/10.5194/essd-7-275-2015.

Gitau, W., P. Camberlin, L. Ogallo, and R. Okoola, 2015: Oceanic and atmospheric linkages with short rainfall season intraseasonal statistics over equatorial eastern Africa and their predictive potential. *Int. J. Climatol.*, **35**, 2382–2399, https://doi.org/10.1002/joc.4131.

Haile, M., 2005: Weather patterns, food security and humanitarian response in sub-Saharan Africa. *Philos. Trans. Roy. Soc. London*, **B360**, 2169–2182, https://doi.org/10.1098/rstb.2005.1746.

Hanssen, A. W., and W. J. A. Kuipers, 1965: On the relationship between the frequency of rain and various meteorological parameters. *K. Ned. Meteor. Inst. M*eded. *Verh.*, **81**, 2–15.

Harvey, L. O., K. R. Hammond, C. M. Lusk, and E. F. Mross, 1992: The application of signal detection theory to weather forecasting behavior. *Mon. Wea. Rev.*, **120**, 863–883, https://doi.org/10.1175/1520-0493(1992)120<0863:TAOSDT>2.0.CO;2.

Hillier, D., and B. Dempsey, 2012: A dangerous delay: The cost of late response to early warnings in the 2011 drought in the Horn of Africa. Save the Children and Oxfam Joint Agency Briefing Paper, 34 pp., http://oxfamilibrary.openrepository.com/oxfam/bitstream/10546/203389/8/bp-dangerous-delay-horn-africa-drought-180112-en.pdf.

Indeje, M., F. H. Semazzi, and L. A. Ogallo, 2000: ENSO signals in East African rainfall seasons. *Int. J. Climatol.*, **20**, 19–46, https://doi.org/10.1002/(SICI)1097-0088(200001)20:1<19::AID-JOC449>3.0.CO;2-0.

Jia, J., and Coauthors, 2015: Improved seasonal prediction of temperature and precipitation over land in a high-resolution GFDL climate model. *J. Climate*, **28**, 2044–2062, https://doi.org/10.1175/JCLI-D-14-00112.1.

Johansson, B., and D. Chen, 2003: The influence of wind and topography on precipitation distribution in Sweden: Statistical analysis and modelling. *Int. J. Climatol.*, **23**, 1523–1535, https://doi.org/10.1002/joc.951.

Kang, H., K.-H. An, C.-K. Park, A. L. S. Solis, and K. Stitthichivapak, 2007: Multimodel output statistical downscaling prediction of precipitation in the Philippines and Thailand. *Geophys. Res. Lett.*, **34**, L15710, https://doi.org/10.1029/2007GL030730.

——, C.-K. Park, S. N. Hameed, and K. Ashok, 2009: Statistical downscaling of precipitation in Korea using multimodel output variables as predictors. *Mon. Wea. Rev.*, **137**, 1928–1938, https://doi.org/10.1175/2008MWR2706.1.

Kharin, V., and F. Zwiers, 2003: On the ROC score of probability forecasts. *J. Climate*, **16**, 4145–4150, https://doi.org/10.1175/1520-0442(2003)016<4145:OTRSOP>2.0.CO;2.

Kipkogei, O., A. Bhardwaj, V. Kumar, L. A. Ogallo, F. J. Opijah, J. N. Mutemi, and T. N. Krishnamurti, 2016: Improving multimodel medium range forecasts over the Greater Horn of Africa using the FSU superensemble. *Meteor. Atmos. Phys.*, **128**, 441–451, https://doi.org/10.1007/s00703-015-0430-0.

Kirtman, B. P., and Coauthors, 2014: The North American Multimodel Ensemble: Phase-1 seasonal-to-interannual prediction; phase-2 toward developing intraseasonal prediction. *Bull.*

Amer. Meteor. Soc., **96**, 686–601, https://doi.org/10.1175/BAMS-D-12-00050.1.

Kumar, K., B. Rajagopalan, and M. Cane, 1999: On the weakening relationship between the Indian monsoon and ENSO. *Science*, **284**, 2156–2159, https://doi.org/10.1126/science.284.5423.2156.

Liu, J., D. Yuan, L. Zhang, X. Zou, and X. Song, 2015: Comparison of three statistical downscaling methods and ensemble downscaling method based on Bayesian model averaging in upper Hanjiang River Basin, China. *Adv. Meteor.*, 7463963, http://dx.doi.org/10.1155/2016/7463963.

Lott, F., and M. J. Miller, 1997: A new subgrid-scale orographic drag parameterization: Its performance and testing. *Quart. J. Roy. Meteor. Soc.*, **123**, 101–127, https://doi.org/10.1002/qj.49712353704.

Marchant, R., C. Mumbi, S. Behera, and T. Yamagata, 2007: The Indian Ocean dipole—The unsung driver of climatic variability in East Africa. *Afr. J. Ecol.*, **45**, 4–16, https://doi.org/10.1111/j.1365-2028.2006.00707.x.

Mason, I., 1982: A model for assessment of weather forecasts. *Aust. Meteor. Mag.*, **30**, 291–303.

Mason, S. J., and S. Chidzambwa, 2008: Verification of African RCOF forecasts. WMO Tech. Rep. 09-02, 26 pp.

——, and N. E. Graham, 1999: Conditional probabilities, relative operating characteristics, and relative operating levels. *Wea. Forecasting*, **14**, 713–725, https://doi.org/10.1175/1520-0434(1999)014<0713:CPROCA>2.0.CO;2.

——, and ——, 2002: Areas beneath the relative operating characteristics (ROC), and relative operating levels (ROL) curves: Statistical significance and interpretation. *Quart. J. Roy. Meteor. Soc.*, **128**, 2145–2166, https://doi.org/10.1256/003590002320603584.

——, and G. M. Mimmack, 2002: Comparison of some statistical methods of probabilistic forecasting of ENSO. *J. Climate*, **15**, 8–29, https://doi.org/10.1175/1520-0442(2002)015<0008:COSSMO>2.0.CO;2.

——, and A. P. Weigel, 2009: A generic forecast verification framework for administrative purposes. *Mon. Wea. Rev.*, **137**, 331–349, https://doi.org/10.1175/2008MWR2553.1.

——, and M. K. Tippett, 2016: Climate predictability tool version 15.3. International Research Institute for Climate and Society, Columbia University, http://doi.org/10.7916/D8NS0TQ6.

——, and ——, 2017: Climate predictability tool version 15.5.10. International Research Institute for Climate and Society, Columbia University, https://doi.org/10.7916/D8G44WJ6.

Michaelsen, J., 1987: Cross-validation in statistical climate forecast models. *J. Climate Appl. Meteor.*, **26**, 1589–1600, https://doi.org/10.1175/1520-0450(1987)026<1589:CVISCF>2.0.CO;2.

Milonov, D., and M. Raschendorfer, 2001: Evaluation of empirical parameters of the new LM surface layer parameterization scheme: Results from numerical experiments including soil moisture analysis. DWD COSMO Tech. Rep. 1, 13 pp., http://www.cosmo-model.org/content/model/documentation/techReports/docs/techReport01.pdf.

Mutai, C. C., M. N. Ward, and A. W. Colman, 1998: Towards the prediction of the East Africa short rains based on sea-surface temperature–atmosphere coupling. *Int. J. Climatol.*, **18**, 975–997, https://doi.org/10.1002/(SICI)1097-0088(199807)18:9<975::AID-JOC259>3.0.CO;2-U.

Mwangi, E., F. Wetterhall, E. Dutra, F. Di Giuseppe, and F. Pappenberger, 2014: Forecasting droughts in East Africa. *Hydrol. Earth Syst. Sci.*, **18**, 611, https://doi.org/10.5194/hess-18-611-2014.

Ndiaye, O., L. Goddard, and M. N. Ward, 2009: Using regional wind fields to improve general circulation model forecasts of July–September Sahel rainfall. *Int. J. Climatol.*, **29**, 1262–1275, https://doi.org/10.1002/joc.1767.

Nicholls, N., 1987: The use of canonical correlation to study teleconnections. *Mon. Wea. Rev.*, **115**, 393–399, https://doi.org/10.1175/1520-0493(1987)115<0393:TUOCCT>2.0.CO;2.

Nicholson, S. E., 2003: Comments on "The South Indian Convergence Zone and interannual rainfall variability over southern Africa" and the question of ENSO's influence on southern Africa. *J. Climate*, **16**, 555–562, https://doi.org/10.1175/1520-0442(2003)016<0555:COTSIC>2.0.CO;2.

——, 2014: The predictability of rainfall over the Greater Horn of Africa. Part I: Prediction of seasonal rainfall. *J. Hydrometeor.*, **15**, 1011–1027, https://doi.org/10.1175/JHM-D-13-062.1.

Okoola, R. E., 1999: Midtropospheric circulation patterns associated with extreme dry and wet episodes over equatorial eastern Africa during the Northern Hemisphere spring. *J. Appl. Meteor.*, **38**, 1161–1169, https://doi.org/10.1175/1520-0450(1999)038<1161:MCPAWE>2.0.CO;2.

Owiti, Z., L. A. Ogallo, and J. Mutemi, 2008: Linkages between the Indian Ocean dipole and East African seasonal rainfall anomalies. *J. Kenya Meteor. Soc.*, **2**, 3–17.

Repelli, C. A., and J. M. B. Alves, 1996: Use of canonical correlation analysis to predict the spatial rainfall variability over the northeast Brazil region. *J. Braz. Meteor. Soc.*, **11**, 67–75.

Rowell, D. P., B. B. B. Booth, S. E. Nicholson, and P. Good, 2015: Reconciling past and future rainfall trends over East Africa. *J. Climate*, **28**, 9768–9788, https://doi.org/10.1175/JCLI-D-15-0140.1.

——, C. A. Senior, M. Vellinga, and R. J. Graham, 2016: Can climate projection uncertainty be constrained over Africa using metrics of contemporary performance? *Climatic Change*, **134**, 621–633, https://doi.org/10.1007/s10584-015-1554-4.

Saha, S., and Coauthors, 2006: The NCEP Climate Forecast System. *J. Climate*, **19**, 3483–3517, https://doi.org/10.1175/JCLI3812.1.

——, and Coauthors, 2010: The NCEP Climate Forecast System Reanalysis. *Bull. Amer. Meteor. Soc.*, **91**, 1015–1067, https://doi.org/10.1175/2010BAMS3001.1.

——, and Coauthors, 2014: The NCEP Climate Forecast System version 2. *J. Climate*, **27**, 2185–2208, https://doi.org/10.1175/JCLI-D-12-00823.1.

Saji, N. H., B. N. Goswanmi, P. N. Vanayachandran, and T. Yamagata, 1999: A dipole mode in the tropical Indian Ocean. *Nature*, **401**, 360–363.

Shanko, D., and P. Camberlin, 1998: The effects of the southwest Indian Ocean tropical cyclones on Ethiopian drought. *Int. J. Climatol.*, **18**, 1373–1388, https://doi.org/10.1002/(SICI)1097-0088(1998100)18:12<1373::AID-JOC313>3.0.CO;2-K.

Smith, R. S., J. Brolley, J. J. O'Brien, and C. A. Tartaglione, 2007: ENSO's impact on regional U.S. hurricane activity. *J. Climate*, **20**, 1404–1414, https://doi.org/10.1175/JCLI4063.1.

Shukla, S., C. Funk, and A. Hoell, 2014: Using constructed analogs to improve the skill of National Multi-Model Ensemble March–April–May precipitation forecasts in equatorial East Africa. *Environ. Res. Lett.*, **9**, 094009, https://doi.org/10.1088/1748-9326/9/9/094009.

Swets, J. A., 1973: The relative operating characteristic in psychology. *Science*, **182**, 990–1000, https://doi.org/10.1126/science.182.4116.990.

Tatsuoka, M. M., 1988: *Multivariate Analysis: Techniques for Educational and Psychological Research*. Macmillan, 479 pp.

Terray, P., and S. Dominiak, 2005: Indian Ocean sea surface temperature and El Niño–Southern Oscillation: A new perspective. *J. Climate*, **18**, 1351–1368, https://doi.org/10.1175/JCLI3338.1.

Vecchi, G. A., and Coauthors, 2014: On the seasonal forecasting of regional tropical cyclone activity. *J. Climate*, **27**, 7994–8016, https://doi.org/10.1175/JCLI-D-14-00158.1.

Washington, R., and T. E. Downing, 1999: Seasonal forecasting of African rainfall: Prediction, responses and household food security. *Geogr. J.*, **165**, 266–274.

Wilby, R. L., and T. M. L. Wigley, 1997: Downscaling general circulation model output: A review of methods and limitations. *Prog. Phys. Geogr.*, **21**, 530–548, https://doi.org/10.1177/030913339702100403.

——, H. Hassan, and K. Hanaki, 1998: Statistical downscaling of hydrometeorological variables using general circulation model output. *J. Hydrol.*, **205**, 1–19, https://doi.org/10.1016/S0022-1694(97)00130-3.

——, C. W. Dawson, and E. M. Barrow, 2002: SDSM—A decision support tool for the assessment of regional climate change impacts. *Environ. Modell. Software*, **17**, 145–157, https://doi.org/10.1016/S1364-8152(01)00060-3.

Wilks, D. S., 1995: *Statistical Methods in the Atmospheric Sciences: An Introduction.* Academic Press, 467 pp.

——, 2006: Canonical correlation analysis. *Statistical Methods in the Atmospheric Sciences*, 2nd ed. J. Hele, Ed., Academic Press, 509–528.

Wu, X., K. S. Moorthi, K. Okamoto, and H. L. Pan, 2005: Sea ice impacts on GFS forecasts at high latitudes. *Eighth Conf. on Polar Meteorology and Oceanography*, San Diego, CA, Amer. Meteor. Soc., 7.4, https://ams.confex.com/ams/pdfpapers/84292.pdf.

Yun, W. T., L. Stefanova, and T. N. Krishnamurti, 2003: Improvement of the multimodel superensemble technique for seasonal forecasts. *J. Climate*, **16**, 3834–3840, https://doi.org/10.1175/1520-0442(2003)016<3834:IOTMST>2.0.CO;2.

Zheng, X., and J. A. Renwick, 2003: A regression-based scheme for seasonal forecasting of New Zealand temperature. *J. Climate*, **16**, 1843–1853, https://doi.org/10.1175/1520-0442(2003)016<1843:ARSFSF>2.0.CO;2.